nanomaterials

MDPI

Communication

A Polyol-Mediated Fluoride Ions Slow-Releasing Strategy for the Phase-Controlled Synthesis of Photofunctional Mesocrystals

Xianghong He *, Yaheng Zhang, Yu Fu, Ning Lian and Zhongchun Li

School of Chemistry and Environmental Engineering, Jiangsu University of Technology, Changzhou 213001, Jiangsu, China; Zhangyaheng@jsut.edu.cn (Y.Z.); fuyu@jsut.edu.cn (Y.F.); ln@jstu.edu.cn (N.L.); lizc@jstu.edu.cn (Z.L.)

* Correspondence: hexh@jsut.edu.cn; Tel.: +86-519-8695-3269

Received: 1 December 2018; Accepted: 22 December 2018; Published: 26 December 2018

Abstract: There are only a few inorganic compounds that have evoked as much interest as sodium yttrium fluoride ($NaYF_4$). Its extensive applications in various fields, including transparent displays, luminescence coding, data storage, as well as biological imaging, demand the precise tuning of the crystal phase. Controlling the emergence of the desired α-phase has so far remained a formidable challenge, especially via a simple procedure. Herein, we represented a polyol-assisted fluoride ions slow-release strategy for the rational control of pure cubic phase $NaYF_4$ mesocrystals. The combination of fluorine-containing ionic liquid as a fluoride source and the existence of a polyalcohol as the reactive medium ensure the formation of uniform α-phase mesocrystallines in spite of a higher temperature and/or higher doping level.

Keywords: polyol-assisted fluoride ions slow-release strategy; $NaYF_4$ mesocrystals; crystallographic phase control

1. Introduction

Since inorganic micro/nanocrystals usually exist in various forms or phases, the phase transformation from kinetically stable ones to thermally stable ones is a normal phenomenon [1–4]. The intrinsic properties of a micro/nanomaterial are largely determined by its unique crystal structure [5,6]. Hence, controlling the phase formation is essential for both scientific interests and extended applications. As a typical example, sodium yttrium fluoride ($NaYF_4$) owns two polymorphs under ambient condition, i.e., the cubic (α-) and hexagonal (β-) phase, which is a commonly used matrix lattice for up-conversion luminescence. The former is a high-temperature metastable phase, while the latter remains thermodynamically stable [7,8]. The past decades have witnessed much exploration of its controlled synthesis and up-/down-conversion luminescent properties [1,4,9–34]. Compared with considerable work on α→β phase transformation [1,4,9–19], the fabrication of α-$NaYF_4$ as well as the investigation involving the β→α transformation process have been neglected [26,30,33,34]. So far, some strategies have been developed to fabricate α-phase $NaYF_4$ nano-/mocro-crystal, such as a liquid–solid–solution (LSS) procedure [21], polyol method [22], two-phase interfacial route [23], microwave-assisted ionic liquid (IL)-based technique [24], modified solvothermal approach [25], and self-sacrificing template multiple-step route [26,27]. Furthermore, introducing Mn^{2+} (r = 81 pm) with a smaller size than Y^{3+} (r = 89 pm) into an $NaYF_4$ host can dominate, forming pure α-phase $NaYF_4$ nanoparticles [28]. However, α-phase $NaYF_4$ inevitably transforms into the hexagonal ones due to its thermodynamic instability. Additionally, the cubic $NaYF_4$ nanoparticles are usually formed preferentially in the solution system of non-equilibrium reactions [20]. As a consequence, rationally

controlling α-$NaYF_4$ and simultaneously avoiding the generation of β-phase or a mixture of α and β phases remain formidable challenges, especially via a simple procedure [28,29,34].

On the other hand, the above-mentioned progress focused on $NaYF_4$ micro/nanocrystals instead of mesocrystals. Mesocrystals are three-dimensional (3D) order nanoparticles superstructures with unique properties and various potential applications as functional materials [35–38]. Nevertheless, the range of known mesocrystallines remains quite limited, in which few investigations to fluorine-containing compound mesocrystallines are available [39–45]. More recently, our group fabricated yttrium hydroxide fluoride mesocrystalline, as well as its Eu^{3+} doped analogue, by means of an additive-free hydrothermal procedure, which involved the reaction of $Y(NO_3)_3$, NaF, and NaOH aqueous solution without any organic additives [39]. Furthermore, we explored the preparation of rare-earths trifluoride mesocrystals by a solvothermal route involving IL 1-butyl-3-methylimidazolium hexafluorophosphate ($BmimPF_6$) as the fluorine source in the presence of 1,4-butanediol [40]. However, no effort has been made to reveal the phase control related to rare-earths fluoride mesocrystallines. Herein, we present a facile, one-pot route called a polyol-mediated fluoride slow-releasing strategy for the rational control of pure phase α-$NaYF_4$ mesocrystals. In spite of a higher temperature or/and higher doping level, cubic phase can be maintained.

2. Experimental Procedure

2.1. Chemicals and Materials

Analytical grade rare earth chlorides and/or nitrates (yttrium chloride hexahydrate, gadolinium chloride hexahydrate, ytterbium nitrate pentahydrate, and erbium nitrate pentahydrate, 99.9%) were provided by Aladdin Industrial Inc. Shanghai, China. $NaNO_3$ (99.0%), 2,2′-oxydiethanol (99.0%, diethylene glycol, abbreviated as DEG), 1,2-ethanediol (99.0%), and ethanol (99.8%) were obtained from Sinopharm Chemical Reagent Company, Shanghai, China. 1-Butyl-3-methylimidazolium hexafluorophosphate ($BminPF_6$, 99%) was purchased from Aldamas-beta Co., Shanghai, China. All of the reagents and solvents were directly used without further treatment.

2.2. Synthesis

$NaYF_4$:Yb^{3+},Er^{3+}(20/2 mol%) (abbreviated as NYF:Yb^{3+},Er^{3+} hereafter) and Gd^{3+} tri-doped NYF:Yb^{3+},Er^{3+}(20/2 mol%) nanocrystals (NCs) were synthesized via a polyol-mediated solvothermal procedure. Here, we took the synthesis of NYF:Yb^{3+},Er^{3+} (20/2 mol%) as an example. The starting chemicals including $NaNO_3$, yttrium chloride hexahydrate, ytterbium nitrate pentahydrate, and erbium nitrate pentahydrate in the stoichiometric ratio were well mixed with 1,2-ethanediol (or DEG) under stirring, to form solution. Thereafter, the solution was slowly added into a 25-mL polytetrafluoroethylene (PTFE) vial containing a proper amount of $BminPF_6$ under vigorous stirring. The autoclave was sealed after vigorous stirring at room temperature for around 15 min, and then heated at 120 °C for 24 h. The final products were collected by centrifugation, and then washed sequentially using ethanol and H_2O three times. After drying at 70 °C under dynamic vacuum for 24 h, an NYF:Yb^{3+},Er^{3+} sample was obtained. The synthetic procedure of Gd^{3+} tri-doped NYF:Yb^{3+},Er^{3+} (20/2 mol%) NCs was the same as that which was used to fabricate NYF:Yb^{3+},Er^{3+}, except that the stoichiometric amount of gadolinium chloride hexahydrate was also added to 1,2-ethanediol (or DEG).

2.3. Characterization

The crystal structure and phase analysis were determined via X-ray diffraction (XRD) using a Bruker D8 Advanced X-ray diffractometer (Ni filtered, Cu K_α radiation, 40 kV and 40 mA) (Bruker, Billerica, MA, USA). The morphology the products were recorded on a transmission electron microscope (TEM, JEM-2010, JOEL Ltd., Tokyo, Japan) and a Hitachi S4800 field-emission scanning electron microscope (FE-SEM) (Hitachi Ltd., Tokyo, Japan). The selected area electron diffraction (SAED) pattern were characterized by the above-mentioned TEM (JEM-2010). An up-conversion

fluorescence spectrum was obtained on an Edinburgh Instrument FLS920 phosphorimeter (Edinburgh Instruments Ltd., Livingston, UK) with a 980-nm laser diode Module (K98D08M-30mW, Changchun, China) as the excitation light source. The above-mentioned measurements were performed at room temperature from powder samples.

3. Results and Discussion

$NaYF_4$-based mesocrystals were fabricated via solvothermal treatment of Na^+, Y^{3+}, and $BminPF_6$ in the presence of viscous polyol-like diethylcol or 1,2-ethanediol. Apart from serving as solvent and complexant (i.e., bonding with Na^+ and Y^{3+}), polyol also acts as a stabilizer that limits particle growth and suppresses the α→β phase transition of $NaYF_4$ [22,46]. $BmimPF_6$ was chosen as a task-specific fluorine source (the reason why it was chosen as the fluorine source is given in the Supplementary Materials). The required fluoride anion (F^-) was provided by $BmimPF_6$ as a result of its slow decomposition and hydrolysis [23,45,47]. Even without additional water, $BmimPF_6$ can hydrolyze with the aid of the trace water and hydration water molecules from yttrium chloride hexahydrate [45,48]. During the treatment procedure, ${PF_6}^-$ can slowly hydrolyze and then produce F^- through slowly increasing the temperature [45], as revealed in Equation (1):

$$ {PF_6}^- \text{ (IL)} + H_2O \rightarrow PF_5{\cdot}H_2O + F^- \quad (1) $$

Therefore, this procedure was defined as a fluoride slow-release strategy, which involved fluoride releasing from $BmimPF_6$ with the assistance of polyol [49].

Powder XRD patterns of a Yb^{3+}-Er^{3+} co-doped and pure $NaYF_4$ submicrocube in the case of DEG as the reaction medium are illustrated in Figures 1a and 2a, respectively. All of the diffraction peaks matched the α-phase $NaYF_4$ crystals (PDF No.77-2042), and no impurities were found. The sharp and narrow diffraction peaks revealled the highly crystallinity of these submicrocubes despite treatment at relatively low temperature (120 °C).

As exhibited in Figure 1b–d, all of the NYF:Yb^{3+},Er^{3+} submicrocrystals show cubic shapes and edge lengths of about 120 nm. Both FE-SEM and TEM photos illustrated their novel microstructure features, which are built from many nanoparticles and exhibited rough surfaces. A few nanoparticles were found attached on its surface (Figure 1e). Especially, the SAED pattern (Figure 1f) of a single $NaYF_4$ cube shows sharp and periodic spots, revealing its noticeable single crystal-like feature. According to Cölfen et al. [35–40], the regular-shaped $NaYF_4$ cubes actually belong to typical mesocrystals. The combination of a coarse surface pattern and the attachment of nanoparticles reveal that these mesocrystallines resulted from the self-assembling of nanoparticle subunits rather than the classic crystalline growth [18,35–40].

When DEG was replaced by 1,2-ethanediol, the product can also be indexed as pure-phase cubic $NaYF_4$ crystal (Figure 2b). All of these results indicated that IL $BmimPF_6$ in the presence of polyol also acts as a crystal-phase manipulator during the formation of $NaYF_4$ [18].

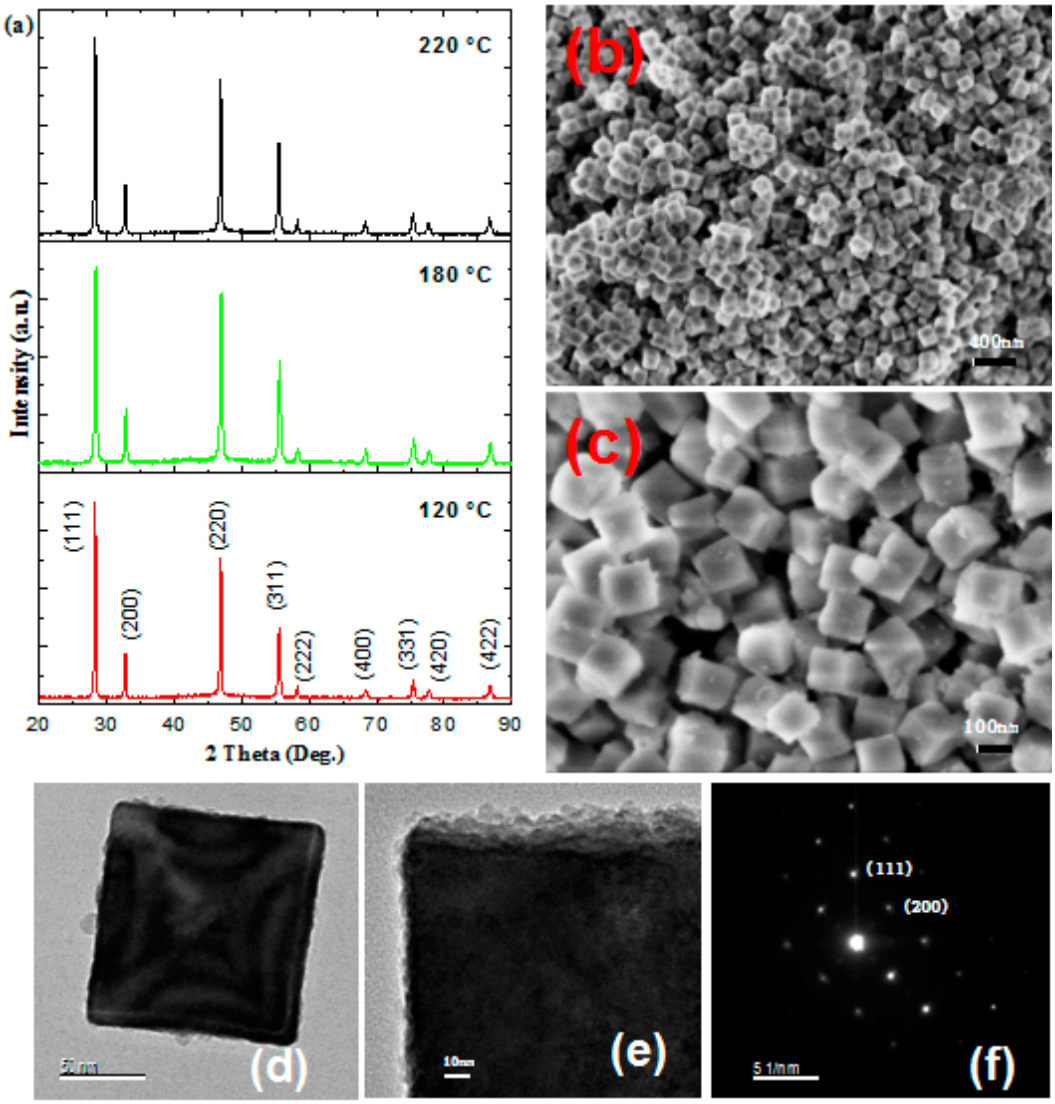

Figure 1. (**a**) X-ray diffraction (XRD) patterns of sodium yttrium fluoride (NYF):$Yb^{3+}Er^{3+}$ (20/2 mol%) sample at various solvothermal temperatures using diethylene glycol (DEG) as the reaction medium (all of the diffraction peaks are attributed to cubic-phase $NaYF_4$), field-emission scanning electron microscope (FE-SEM) images ((**b**) low-magnification; (**c**) high-magnification), (**d**,**e**) TEM images, and (**f**) selected area electron diffraction (SAED) pattern of as-obtained NYF:Yb^{3+},Er^{3+} (20/2 mol%) submicrocrystals at 120 °C. (Note the nanoparticles aggregated to form submicrocubes).

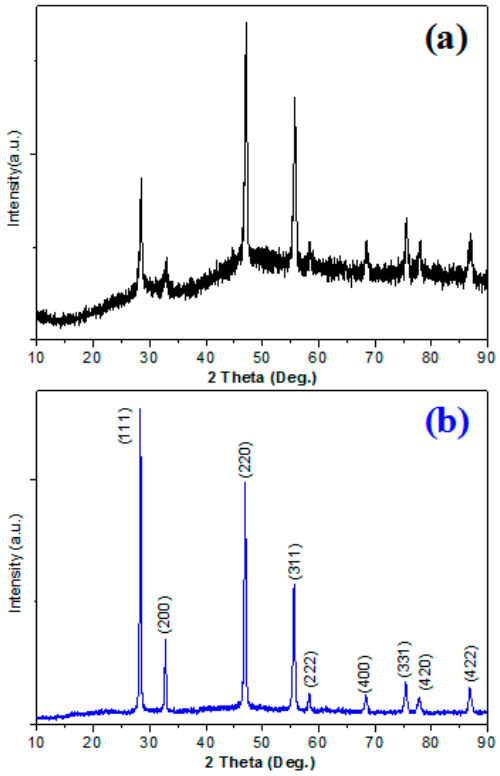

Figure 2. XRD patterns of (**a**) $NaYF_4$ host, and (**b**) NYF:Yb^{3+},Er^{3+} (20/2 mol%) samples using 1,2-ethanediol as solvent.

For comparison, the preparation of NYF:Yb^{3+},Er^{3+} was also conducted through an LSS procedure using NH_4F as the F^- source and the mixture of ethanol–H_2O–oleic acid as the medium at 120 °C and 220 °C [11,21]. Figure S2 (see Supplementary Materials) revealed the XRD patterns of as-obtained NYF:Yb^{3+},Er^{3+} (20/2 mol%) at 120 °C and 220 °C. Obviously, the product obtained at the lower temperature can be ascribed to a pure α-phase $NaYF_4$, as expected for $NaYF_4$ synthesized under mild conditions [21,23,32]. However, in the case of higher temperature (220 °C), only β-phase $NaYF_4$ was fabricated. These results demonstrated that promoting the reaction temperature can induce the α→β phase change of $NaYF_4$, which is consistent with previous reports [9–12]. However, as shown in Figure 1a, even if the reaction temperature reached 220 °C, the as-prepared nanoparticles via the fluoride ions-slow-release procedure unambiguously remained in a pure cubic phase. In a word, regardless of the treatment temperature, an α-phase $NaYF_4$ can be obtained by this slow-release strategy.

As mentioned above, without the tri-doping of Gd^{3+}, the XRD pattern of the NYF:Yb^{3+},Er^{3+} (20/2 mol%) sample matched a cubic phase of $NaYF_4$ (PDF No.77-2042). As for the NYF:Yb^{3+},Er^{3+} (20/2 mol%) sample, previous works revealed that introducing lanthanide ions (such as Gd^{3+}) with a larger size than the Y^{3+} ion in the $NaYF_4$ lattice not only induced an alteration from the α phase to the β phase, it also dominated the forming of pure β-phase $NaYF_4$ NCs [1,20,50]. However, in this work, as revealed in Figure 3a, the pure cubic phase of $NaYF_4$ remained when Gd^{3+} of 15 mol% was incorporated into host lattices. With the further increasing of the Gd^{3+} ion content (Figure 3b), no impurity diffraction peaks were found, showing the forming of a homogeneous solid solution, which is due to the small structural difference between the cubic-phase $NaGdF_4$ and $NaYF_4$. Obviously, phase transformation did not occur upon a higher-level doping of the dopant.

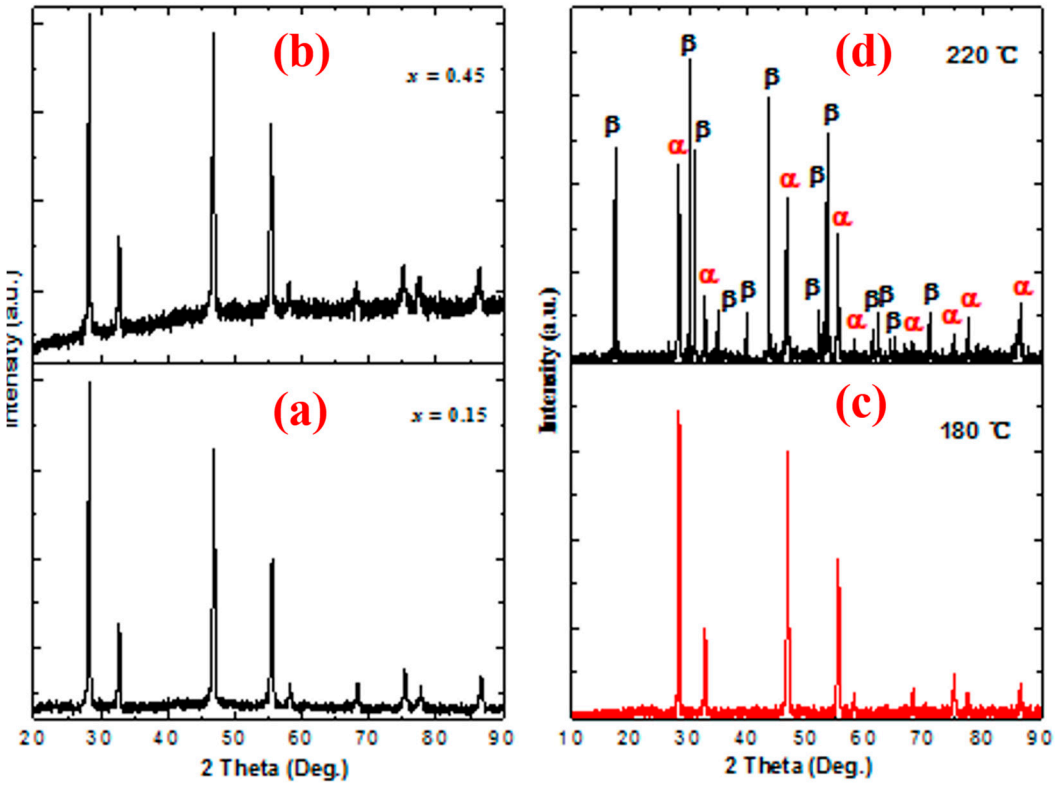

Figure 3. XRD patterns of Na ($Y_{0.78-x}Gd_x$), F_4:Yb^{3+}, and Er^{3+}(20/2 mol%) samples with different tri-doping levels of Gd^{3+} ((**a**) x = 0.15, (**b**) x = 0.45), and Na ($Y_{0.48}Gd_{0.30}$)F_4:Yb^{3+},Er^{3+}(20/2 mol%) samples obtained at higher solvothermal temperatures ((**c**) 180 °C, (**d**) 220 °C; the symbol α and β represent cubic and hexagonal phases, respectively).

High-level doping usually leads to an α→β phase transition of $NaYF_4$ in the LSS reaction system [1,20]. However, in present work, by using $BminPF_6$ and polyol as the F^- source and reaction medium, respectively, as shown in Figure 3c, the as-synthesized submicrocubes remained in the cubic phase of $NaYF_4$ in spite of higher total doping concentrations (52 mol%) as well as a higher solvothermal treatment temperature (180 °C). Even if the total doping contents were set as high as 52 mol%, and the treatment temperature simultaneously approached 220 °C (near to the work-limited temperature of the PTFE vial), the α-phase $NaYF_4$ still existed in the products (see Figure 3d).

According to He et al. [51], the α→β phase change of $NaYF_4$ can be attributed to the elevated content of F^- and the alteration to the reaction environment of Y^{3+} ions. In an LSS system involving oleic acid and a high active F^- source such as NH_4F and NaF, it is found that the oleate anions are more likely to be combined with Y^{3+} in comparison with Na^+ ions [4]. The interaction between oleate anions and Y^{3+} could effectively lower the energy barrier of the α→β phase transition [4]. Moreover, effective concentration of F^- ions was elevated, resulting from the rapid supply of F^-. All of these could effectively promote the α→β phase transformation of $NaYF_4$ [4,52,53]. Ultimately, β-phase $NaYF_4$ was formed in an LSS system [9–12,21].

However, in the case of $BminPF_6$ as the F^- source in the presence of polyol, the interaction between PF_6^- ions and Y^{3+} was quite limited compared with the case of the above-mentioned LSS system [17,18]. In addition, noting the solubility product of $NaYF_4$, $a_{Na}a_Ya_F{}^4$, the supersaturation degree ($a_{Na}a_Ya_F{}^4/K_{SP}$) drastically varies with the content of fluoride ions, with an exponential relationship. Thus, the content of fluoride ions in a reactive system is of importance to the phase control of $NaYF_4$ [15,19,33]. Herein, $BmimPF_6$ slowly decomposes and hydrolyzes to create the required F^- during the elevation of the reaction temperature [23,45,47]. Therefore, $BmimPF_6$ is a low-active F^- source relative to NH_4F and NaF. Since the equilibrium constant of the hydrolyzed reaction (Equation (1)) is extremely small, the effective concentration of F^- ions was relatively low in

the reaction system, which consequently results in a very slow precipitation with Na^+ and Y^{3+} [45] (Equation (2)).

$$Na^+ + Y^{3+} + 4F^- \rightarrow NaYF_4 \downarrow \quad (2)$$

In such circumstances, the supersaturation degree of the reaction system is not adequate to form the nuclei of the hexagonal phase $NaYF_4$ [23]. Therefore, the formation of cubic phase $NaYF_4$ was favored [51].

As mentioned above, polyol can complex with Na^+ and Y^{3+}. In addition, according to Chaumont et al. [54], PF_6^- (IL) can coordinate with Y^{3+}. Consequently, when $BmimPF_6$ was uniformly dispersed in 1,2-ethanediol (or DEG) solution containing Na^+ and Y^{3+} ions, these metal ions were believed to be simultaneously bonded by PF_6^- anions as well as polyol [45]. In this case, Na^+ and Y^{3+} ions were in the same shell surrounded by the imidazolium cation of $BmimPF_6$ [23]. Upon thermal treatment, PF_6^- slowly hydrolyzed and released F^-, which was accompanied by forming $NaYF_4$ nanosized grains; this can be evidenced by the nanoparticles that were attached on the surface of the as-obtained mesocrystals (Figure 1e). Subsequently, the polyol and IL co-stabilized nanoparticles aggregated to form $NaYF_4$ mesocrystals, which possibly occurred through oriented attachment or mesoscale assembly processes due to the coexistence of a Coulombic force, van der Waals interaction, and hydrogen bonds in the system of polyol and $BminPF_6$ [55,56]. Finally, it should be pointed out that the above-proposed forming course is only one of several possible mechanisms. Further studies about this issue are underway, and will be reported in future work.

Under the excitation of a 980-nm laser, α-phase NYF:Yb^{3+},Er^{3+} (20/2 mol%) mesocrystalline emitted bright yellow fluorescence, which demonstrated its photo functionality performance. The related luminescence spectrum is shown in Figure 4a. The green-emitting bands at about 521 nm and 540/552 nm are due to the $^2H_{11/2} \rightarrow {}^4I_{15/2}$ and $^4S_{3/2} \rightarrow {}^4I_{15/2}$ energy-level transitions of Er^{3+}, respectively, while the red band at around 651/669 nm is assigned to the $^4F_{9/2} \rightarrow {}^4I_{15/2}$ transition of Er^{3+}. The related Commission Internationale de l'Eclairage (CIE) coordinates are calculated as (x = 0.3984, y = 0.5854), which are situated in the region of yellowish light (point "×" in Figure 4b), revealing that it emitted yellowish light.

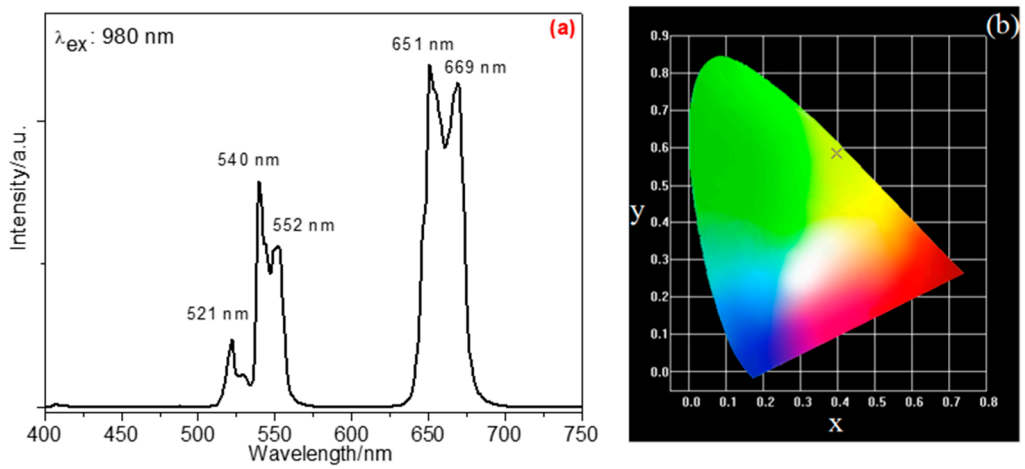

Figure 4. (**a**) Up-conversion luminescence spectrum at room temperature and (**b**) Commission Internationale de l'Eclairage (CIE) chromaticity diagram of NYF:Yb^{3+},Er^{3+}(20/2 mol%) sample (λ_{ex}: 980 nm).

4. Conclusions

In summary, cubic-phase well-defined $NaYF_4$ based photofunctional mesocrystallines were successfully prepared at relatively low temperature by using IL $BmimPF_6$ and viscous polyol as the fluorine source and reaction medium, respectively. Combining slow-releasing fluoride via the decomposition and hydrolysis of fluorine-containing IL and the assistance of polyol, the formation of

cubic-phase $NaYF_4$ was favored, despite the higher treatment temperature or/and higher content of dopant. We believed that the key to the formation of uniform α-$NaYF_4$-based mesocrystals is the use of fluorine-containing IL as a fluorine source as well as the existence of a polyalcohol. Our contribution offers a new alternative in constructing mesocrystal and other hierarchical nanostructured materials with an object phase under mild conditions.

Supplementary Materials: The following are available online at http://www.mdpi.com/2079-4991/9/1/28/s1, Figure S1: XRD pattern of the sample using $BmimBF_4$ as fluorine source (The bar represents the standard cards PDF#70-1935 for YF_3), Figure S2: XRD patterns of NYF:Yb^{3+},Er^{3+} (20/2 mol%) NCs via LSS method at (a) 120 °C and (b) 220 °C (The bars in (a) and (b) represent the standard cards PDF#77-2042 and #PDF16-0334, respectively).

Author Contributions: Supervision, X.H.; data curation, X.H.; writing—original draft preparation, X.H.; writing—review and editing, Y.Z.; investigation, Y.F.; formal analysis, N.L.; methodology, Z.L.

Funding: This research was funded by the National Natural Science Foundation of China, grant number 51872129; and the Natural Science Research Fund of Jiangsu University of Technology.

Conflicts of Interest: The authors declare no conflict of interest.

References

1. Wang, F.; Han, Y.; Lim, C.; Lu, Y.; Wang, J.; Xu, J.; Chen, H.; Zhang, C.; Hong, M.; Liu, X.G. Simultaneous phase and size control of upconversion nanocrystals through lanthanide doping. *Nature* **2010**, *463*, 1061–1065. [CrossRef] [PubMed]
2. Farvid, S.S.; Radovanovic, P.V. Phase Transformation of Colloidal In_2O_3 Nanocrystals Driven by the Interface Nucleation Mechanism: A Kinetic Study. *J. Am. Chem. Soc.* **2012**, *134*, 7015–7024. [CrossRef] [PubMed]
3. Song, S.; Kuang, Y.; Liu, J.; Yang, Q.; Luo, L.; Sun, X. Separation and phase transition investigation of Yb^{3+}/Er^{3+} co-doped $NaYF_4$ nanoparticles. *Dalton Trans.* **2013**, *42*, 13315–13318. [CrossRef] [PubMed]
4. Sui, Y.Q.; Tao, K.; Tian, Q.; Sun, K. Interaction between Y^{3+} and Oleate Ions for the Cubic-to-Hexagonal Phase Transformation of $NaYF_4$ Nanocrystals. *J. Phys. Chem. C* **2012**, *116*, 1732–1739. [CrossRef]
5. Zhang, F.; Li, G.; Zhang, W.; Yan, Y.L. Phase-Dependent Enhancement of the Green-Emitting Upconversion Fluorescence in $LaVO_4$:Yb^{3+},Er^{3+}. *Inorg. Chem.* **2015**, *54*, 7325–7334. [CrossRef] [PubMed]
6. Zhua, Y.; Chen, D.; Huang, L.; Liu, Y.; Brikd, M.G.; Zhong, J.; Wang, J. Phase-transition-induced giant enhancement of red emission in Mn^{4+}-doped fluoride elpasolite phosphors. *J. Mater. Chem. C* **2018**, *6*, 3951–3960. [CrossRef]
7. Thoma, R.E.; Hebert, G.M.; Insley, H.; Weaver, C.F. Phase Equilibria in the System Sodium Fluoride-Yttrium Fluoride. *Inorg. Chem.* **1963**, *2*, 1005–1012. [CrossRef]
8. Arnold, A.A.; Terskikh, V.; Li, Q.Y.; Naccache, R.; Marcotte, I.; Capobianco, J. Structure of $NaYF_4$ Upconverting Nanoparticles: A Multinuclear Solid-State NMR and DFT Computational Study. *J. Phys. Chem. C* **2013**, *117*, 25733–25741. [CrossRef]
9. Mai, H.X.; Zhang, Y.W.; Si, R.; Yan, Z.G.; Sun, L.D.; You, L.P.; Yan, C.H. High-Quality Sodium Rare-earth Fluoride Nanocrystals: Controlled Synthesis and Optical Properties. *J. Am. Chem. Soc.* **2006**, *128*, 6426–6436. [CrossRef]
10. Wei, Y.; Lu, F.; Zhang, X.; Chen, D. Synthesis of Oil-Dispersible Hexagonal-Phase and Hexagonal-Shaped $NaYF_4$:Yb,Er Nanoplates. *Chem. Mater.* **2006**, *18*, 5733–5737. [CrossRef]
11. Zhang, F.; Wan, Y.; Yu, T.; Zhang, F.; Shi, Y.; Xie, S.; Li, Y.; Xu, L.; Tu, B.; Zhao, D. Uniform Nanostructured Arrays of Sodium Rare-Earth Fluorides for Highly Efficient Multicolor Upconversion Luminescence. *Angew. Chem. Int. Ed.* **2007**, *46*, 7976–7979. [CrossRef] [PubMed]
12. Wang, L.; Li, Y. Controlled Synthesis and Luminescence of Lanthanide Doped $NaYF_4$ Nanocrystals. *Chem. Mater.* **2007**, *19*, 727–734. [CrossRef]
13. Yi, G.S.; Chow, G.M. Synthesis of Hexagonal-Phase $NaYF_4$:Yb,Er and $NaYF_4$:Yb,Tm Nanocrystals with Efficient Up-Conversion Fluorescence. *Adv. Funct. Mater.* **2006**, *16*, 2324–2329. [CrossRef]
14. Shan, J.; Ju, Y. A Single-Step Synthesis and the Kinetic Mechanism for Monodisperse and Hexagonal-Phase $NaYF_4$:Yb,Er Upconversion Nanophosphors. *Nanotechnology* **2009**, *20*, 275603. [CrossRef] [PubMed]
15. Li, C.; Zhang, C.; Hou, Z.; Wang, L.; Quan, Z.; Lian, H.; Lin, J. β-$NaYF_4$ and β-$NaYF_4$:Eu^{3+} Microstructures: Morphology Control and Tunable Luminescence Properties. *J. Phys. Chem. C* **2009**, *113*, 2332–2339. [CrossRef]

16. Wang, Z.L.; Hao, J.; Chan, H.L.; Wong, W.T.; Wong, K.L. A strategy for simultaneously realizing the cubic-to-hexagonal phase transition and controlling the small size of $NaYF_4$:Yb^{3+},Er^{3+} nanocrystals for in vitro cell imaging. *Small* **2012**, *8*, 1863–1868. [CrossRef] [PubMed]
17. He, M.; Huang, P.; Zhang, C.; Chen, F.; Wang, C.; Ma, J.; He, R.; Cui, D. A general strategy for the synthesis of upconversion rare earth fluoride nanocrystals via a novel OA/ionic liquid two-phase system. *Chem. Commun.* **2011**, *47*, 9510–9512. [CrossRef]
18. He, M.; Huang, P.; Zhang, C.; Ma, J.; He, R.; Cui, D. Phase- and Size-Controllable Synthesis of Hexagonal Upconversion Rare-Earth Fluoride Nanocrystals through an Oleic Acid/Ionic Liquid Two-Phase System. *Chem. Eur. J.* **2012**, *18*, 5954–5969. [CrossRef]
19. Zhang, Q.; Yan, B. Phase control of upconversion nanocrystals and new rare earth fluorides though a diffusion-controlled strategy in a hydrothermal system. *Chem. Commun.* **2011**, *47*, 5867–5869. [CrossRef]
20. Chen, D.; Huang, P.; Yu, Y.; Huang, F.; Yang, A.; Wang, Y. Dopant-induced phase transition: A new strategy of synthesizing hexagonal upconversion $NaYF_4$ at low temperature. *Chem. Commun.* **2011**, *47*, 5801–5803. [CrossRef]
21. Wang, X.; Zhuang, J.; Peng, Q.; Li, Y. A general strategy for nanocrystal synthesis. *Nature* **2005**, *437*, 121–124. [CrossRef] [PubMed]
22. Wei, Y.; Lu, F.; Zhang, X.; Chen, D. Polyol-mediated synthesis and luminescence of lanthanide-doped $NaYF_4$ nanocrystal upconversion phosphors. *J. Alloys Compd.* **2008**, *455*, 376–384. [CrossRef]
23. Zhang, C.; Chen, J. Facile EG/ionic liquid interfacial synthesis of uniform RE^{3+} doped $NaYF_4$ nanocubes. *Chem. Commun.* **2010**, *46*, 592–594. [CrossRef] [PubMed]
24. Chen, C.; Sun, L.D.; Li, Z.X.; Li, L.L.; Zhang, J.; Zhang, Y.W.; Yan, C.H. Ionic Liquid-Based Route to Spherical $NaYF_4$ Nanoclusters with the Assistance of Microwave Radiation and Their Multicolor Upconversion Luminescence. *Langmuir* **2010**, *26*, 8797–8803. [CrossRef] [PubMed]
25. Li, H.; Wang, L. Controllable Multicolor Upconversion Luminescence by Tuning the NaF Dosage. *Chem. Asian J.* **2014**, *9*, 153–157. [CrossRef] [PubMed]
26. Han, Y.; Gai, S.; Ma, P.; Wang, L.; Zhang, M.; Huang, S.; Yang, P. Highly Uniform α-$NaYF_4$:Yb/Er Hollow Microspheres and Their Application as Drug Carrier. *Inorg. Chem.* **2013**, *52*, 9184–9191. [CrossRef] [PubMed]
27. Lv, C.; Di, W.; Liu, Z.; Zheng, K.; Qin, W. Synthesis of $NaLuF_4$-based nanocrystals and large enhancement of upconversion luminescence of $NaLuF_4$:Gd, Yb, Er by coating an active shell for bioimaging. *Dalton Trans.* **2014**, *43*, 14001–14008.
28. Tian, G.; Gu, Z.; Zhou, L.; Yin, W.; Liu, X.; Yan, L.; Zhao, Y. Mn^{2+} Dopant-Controlled Synthesis of $NaYF_4$:Yb/Er Upconversion Nanoparticles for in vivo Imaging and Drug Delivery. *Adv. Mater.* **2012**, *24*, 1226–1231. [CrossRef]
29. Heer, S.; Kömpe, K.; Güdel, H.U.; Haase, M. Highly Efficient Multicolour Upconversion Emission in Transparent Colloids of Lanthanide-Doped $NaYF_4$ Nanocrystals. *Adv. Mater.* **2004**, *16*, 2102–2105. [CrossRef]
30. Gao, L.; Ge, X.; Chai, Z.; Xu, G.; Wang, X.; Wang, C. Shape-controlled synthesis of octahedral α-$NaYF_4$ and its rare earth doped submicrometer particles in acetic acid. *Nano Res.* **2010**, *2*, 565–574. [CrossRef]
31. Liang, X.; Wang, X.; Zhuang, J.; Peng, Q.; Li, Y. Synthesis of $NaYF_4$ Nanocrystals with Predictable Phase and Shape. *Adv. Funct. Mater.* **2007**, *17*, 2757–2765. [CrossRef]
32. Zhang, F.; Li, J.; Shan, J.; Xu, L.; Zhao, D. Shape, Size, and Phase-Controlled Rare-Earth Fluoride Nanocrystals with Optical Up-Conversion Properties. *Chem. Eur. J.* **2009**, *15*, 11010–11019. [CrossRef] [PubMed]
33. Qin, R.; Song, H.; Pan, G.; Zhao, H.; Ren, X.; Liu, L.; Bai, X.; Dai, Q.; Qu, X. Polyol-mediated synthesis of well-dispersed α-$NaYF_4$ nanocubes. *J. Cryst. Growth* **2009**, *311*, 1559–1564. [CrossRef]
34. He, L.; Zou, X.; He, X.; Lei, F.; Jiang, N.; Zheng, Q.; Xu, C.; Liu, Y.; Lin, D. Reducing Grain Size and Enhancing Luminescence of $NaYF_4$:Yb^{3+}, Er^{3+} Upconversion Materials. *Cryst. Growth Des.* **2018**, *18*, 808–817. [CrossRef]
35. Cölfen, H.; Antonietti, M. Mesocrystals: Inorganic superstructures made by highly parallel crystallization and controlled alignment. *Angew. Chem. Int. Ed.* **2005**, *44*, 5576–5591. [CrossRef] [PubMed]
36. Niederberger, M.; Cölfen, H. Oriented attachment and mesocrystals: Non-classical crystallization mechanisms based on nanoparticle assembly. *Phys. Chem. Chem. Phys.* **2006**, *8*, 3271–3287. [CrossRef] [PubMed]
37. Bergström, L.; Sturm (née Rosseeva), E.V.; German, S.; Cölfen, H. Mesocrystals in Biominerals and Colloidal Arrays. *Acc. Chem. Res.* **2015**, *48*, 1391–1402. [CrossRef]

38. Zhou, L.; O'Brien, P. Mesocrystals-Properties and Applications. *J. Phys. Chem. Lett.* **2012**, *3*, 620–628. [CrossRef]
39. He, X.; Yan, B. Yttrium hydroxide fluoride based monodisperse mesocrystals: Additive-free synthesis, enhanced fluorescent properties, and potential application in temperature sensing. *CrystEngComm* **2015**, *17*, 621–627. [CrossRef]
40. He, X.; Yan, B. Double role of the hydroxy group for water dispersibility and luminescence of REF_3 (RE = Yb, Er, Tm) based mesocrystals. *New J. Chem.* **2015**, *39*, 6730–6733. [CrossRef]
41. Zhuang, J.; Yang, X.; Fu, J.; Liang, C.; Wu, M.; Wang, J.; Su, Q. Monodispersed β-$NaYF_4$ Mesocrystals: In Situ Ion Exchange and Multicolor Up-and Down-Conversions. *Cryst. Growth Des.* **2013**, *13*, 2292–2297. [CrossRef]
42. Zhong, S.L.; Lu, Y.; Gao, M.R.; Liu, S.J.; Peng, J.; Zhang, L.C.; Yu, S.H. Monodisperse Mesocrystals of YF_3 and Ce^{3+}/Ln^{3+} (Ln=Tb, Eu) Co-Activated YF_3: Shape Control Synthesis, Luminescent Properties, and Biocompatibility. *Chem. Eur. J.* **2012**, *18*, 5222–5231. [CrossRef] [PubMed]
43. Lausser, C.; Kumke, M.U.; Antonietti, M.; Cölfen, H. Fabrication of EuF_3-Mesocrystals in a Gel Matrix. *Z. Anorg. Allg. Chem.* **2010**, *636*, 1925–1930. [CrossRef]
44. Wang, J.; Liu, B.Q.; Huang, G.; Zhang, Z.J.; Zhao, J.T. Monodisperse $Na_xY(OH)_yF_{3+x-y}$ mesocrystals with tunable morphology and chemical composition: pH-mediated ion-exchange. *Cryst. Growth Des.* **2017**, *17*, 711–718. [CrossRef]
45. Zhang, C.; Chen, J.; Zhou, Y.; Li, D. Ionic liquid-based "all-in-one" synthesis and photoluminescence properties of lanthanide fluorides. *J. Phys. Chem. C* **2008**, *112*, 10083–10088. [CrossRef]
46. Zhao, Q.; You, H.; Lü, W.; Guo, N.; Jia, Y.; Lv, W.; Jiao, M. Dendritic $Y_4O(OH)_9NO_3$:Eu^{3+}/Y_2O_3:Eu^{3+} hierarchical structures: Controlled synthesis, growth mechanism, and luminescence properties. *CrystEngComm* **2013**, *15*, 4844–4851. [CrossRef]
47. Swatloski, R.P.; Holbrey, J.D.; Rogers, R.D. Ionic liquids are not always green: Hydrolysis of 1-butyl-3-methylimidazolium hexafluorophosphate. *Green Chem.* **2003**, *5*, 361–363. [CrossRef]
48. Xie, N.; Luan, W. Ionic-liquid-induced microfluidic reaction for water-soluble $Ce_{1-x}Tb_xF_3$ nanocrystal synthesis. *Nanotechnology* **2011**, *22*, 265609. [CrossRef]
49. Lin, J.; Wang, Q. Systematic studies for the novel synthesis of nano-structured lanthanide fluorides. *Chem. Eng. J.* **2014**, *250*, 190–197. [CrossRef]
50. Klier, D.T.; Kumke, M.U. Upconversion Luminescence Properties of $NaYF_4$:Yb:Er Nanoparticles Codoped with Gd^{3+}. *J. Phys. Chem. C* **2015**, *119*, 3363–3373. [CrossRef]
51. He, M.; Huang, P.; Zhang, C.; Hu, H.; Bao, C.; Gao, G.; He, R.; Cui, D. Dual Phase-Controlled Synthesis of Uniform Lanthanide-Doped $NaGdF_4$ Upconversion Nanocrystals Via an OA/Ionic Liquid Two-Phase System for In Vivo Dual-Modality Imaging. *Adv. Funct. Mater.* **2011**, *21*, 4470–4477. [CrossRef]
52. Ghosh, P.; Patra, A. Tuning of crystal phase and luminescence properties of Eu^{3+} doped sodium yttrium fluoride nanocrystals. *J. Phys. Chem. C* **2008**, *112*, 3223–3231. [CrossRef]
53. Xue, X.; Duan, Z.; Suzuki, T.; Tiwari, R.N.; Yoshimura, M.; Ohishi, Y. Luminescence Properties of α-$NaYF_4$:Nd^{3+} Nanocrystals Dispersed in Liquid: Local Field Effect Investigation. *J. Phys. Chem. C* **2012**, *116*, 22545–22551. [CrossRef]
54. Chaumont, A.; Wipff, G. Solvation of M^{3+} lanthanide cations in room-temperature ionic liquids. A molecular dynamics investigation. *Phys. Chem. Chem. Phys.* **2003**, *5*, 3481–3488. [CrossRef]
55. Yasui, K.; Kato, K. Oriented Attachment of Cubic or Spherical $BaTiO_3$ Nanocrystals by van der Waals Torque. *J. Phys. Chem. C* **2015**, *119*, 24597–24605. [CrossRef]
56. Ye, J.; Liu, W.; Cai, J.; Chen, S.; Zhao, X.; Zhou, H.; Qi, L. Nanoporous anatase TiO_2 mesocrystals: Additive-free synthesis, remarkable crystalline-phase stability, and improved lithium insertion behavior. *J. Am. Chem. Soc.* **2011**, *133*, 933–940. [CrossRef] [PubMed]